The low field microwave effective linewidth in polycrystalline ferrites

Nan Mo,[a] Jerome J. Green, Pavol Krivosik,[b] and Carl E. Patton
Department of Physics, Colorado State University, Fort Collins, Colorado 80523

(Received 25 July 2006; accepted 4 November 2006; published online 25 January 2007)

High precision measurements on the low and high field effective linewidth ΔH_{eff} at 10 GHz have been made on ultradense (UD) and conventionally sintered (CS) polycrystalline yttrium iron garnet (YIG) materials. The high field data confirm previous results on the role of two magnon scattering to low wave number (k) electromagnetic Larmor branch spin waves that lie below the light line. The low field data reveal two important contributions to the effective linewidth. For a field regime from the low k edge of the usual dipole exchange spin wave band down to the point in field ($H=H_X$) where above-the-light-line electromagnetic branch Larmor (EML-HI) spin waves appear, ΔH_{eff} is connected with scattering to relatively high k dipole exchange Larmor (DEL) spin waves. The coupling to these modes comes from grain boundaries in the YIG materials. A grain boundary scattering theory gives reasonable agreement with the data. While the high field effective linewidth due to pseudo in-manifold scattering is larger for the CS samples compared to that for the UD samples, the high k DEL scattering is larger for the UD samples compared to that for the CS samples. This is due to the dominant role of the grain boundaries in the low field ΔH_{eff}. For fields below H_X, additional scattering appears for the EML-HI modes. The abrupt appearance of an additional ΔH_{eff} component for $H<H_X$ provides direct experimental evidence for the presence of such modes in the spin wave dispersion. Part of the loss contribution for $H<H_X$ may be due to subthreshold nonlinear effects. © *2007 American Institute of Physics*. [DOI: 10.1063/1.2426379]

I. INTRODUCTION

In the last decade, an increasing need for low loss polycrystalline ferrite materials for high frequency applications has provided an impetus for renewed work on the fundamental understanding of microwave loss and relaxation, damping processes, and precessional dynamics in such systems. Ferromagnetic resonance (FMR) and the FMR linewidth have long been the mainstay for such work.

In the late 1960s and 1970s, however, there was a gradual realization that the off resonance losses, expressed in terms of an effective linewidth, could be substantially lower than those defined through a single FMR linewidth parameter. Just as the usual field swept FMR linewidth ΔH is an expression of the uniform mode relaxation rate η_0 at resonance, given by $\Delta H=2\eta_0/|\gamma|$ for spherical samples, for example, the effective linewidth ΔH_{eff} expresses the relaxation rate $\eta(H)$ for a general static external magnetic field H in field units according to $\Delta H_{\text{eff}}=2\eta(H)/|\gamma|$. This ΔH_{eff} parameter has proven to be a convenient basis for the comparison of off resonance losses with FMR losses as well as off resonance losses for different materials, microstructures, etc. In the above, γ denotes the electron gyromagnetic ratio of the material of interest. All equations here and below are in Gaussian units.

These H-dependent losses can be extremely important because the now well-accepted two magnon scattering contributions to the microwave losses in many magnetic systems can be field and frequency dependent. Microwave measurements at high or low field, very far from the FMR field for a given drive frequency, correspond to a density of states (DOS) situation for degenerate magnon modes that is very different from the situation at ferromagnetic resonance. There are also many microwave magnetic devices that operate at fields that are very far from the FMR field. The corresponding losses can be quite different from those inferred from a single FMR linewidth parameter.

The basic effective linewidth results from the 1960s and 1970s have stood unchallenged until recent work by Mo *et al.*[1] The old work confirmed four expected effects. (1) The effective linewidth is field dependent. (2) It is large and shows considerable structure in the manifold region, where there are a large number of low wave number spin waves that are degenerate with the driven FMR mode. (3) At very high fields, it is generally much lower than the FMR linewidth and the in-manifold ΔH_{eff}. (4) At H values well below FMR field but still sufficient to achieve a saturated sample, ΔH_{eff} is typically a little higher than the average high field values.

The old data, however, also showed two key contradictions. First, the average high field effective (HFE) linewidth, denoted as $\Delta H_{\text{eff}}^{(\text{HF})}$, was always higher than the corresponding FMR linewidths in single crystals.[2] This is problematic because at high field, the spin wave band is shifted to frequencies that are much higher than the drive frequency, and there should be no two magnon scattering contribution whatsoever to the linewidth. This means that $\Delta H_{\text{eff}}^{(\text{HF})}$ should be identical to the intrinsic single crystal linewidth.[3] Second, $\Delta H_{\text{eff}}^{(\text{HF})}$ was also found to have a strong microstructure dependence.[2,4,5] There are substantial increases in $\Delta H_{\text{eff}}^{(\text{HF})}$

[a]Electronic mail: monan@lamar.colostate.edu
[b]On leave from the Department of Electromagnetic Field Theory, Faculty of Electrical Engineering and Information Technology, Slovak University of Technology, Bratislava, Slovakia.

 © 2007 American Institute of Physics

Downloaded 14 Mar 2007 to 129.82.140.121. Redistribution subject to AIP license or copyright, see http://jap.aip.org/jap/copyright.jsp

with both increasing porosity and decreasing grain size. Both responses are inconsistent with the idea of a high field "intrinsic" loss parameter in the absence of two magnon scattering.

The work in Ref. 1 has resolved many of these contradictions. The authors were able to perform meticulous high accuracy measurements of $\Delta H_{\mathrm{eff}}^{(\mathrm{HF})}$ vs H in both conventionally sintered (CS) and ultrahigh density (UD) hot isostatic pressed (hipped) samples of polycrystalline yttrium iron garnet (YIG) spheres. The data showed that $\Delta H_{\mathrm{eff}}^{(\mathrm{HF})}$ is, in fact, not constant at high field, but instead decreases steadily as the field is increased. Remarkably, $\Delta H_{\mathrm{eff}}^{(\mathrm{HF})}$ approaches single crystal YIG linewidth values in the high field limit. Equally remarkable, Ref. 1 also established a correlation between the $\Delta H_{\mathrm{eff}}^{(\mathrm{HF})}(H)$ response and the field dependent density of states for low wave number electromagnetic spin wave (EMSW) modes. Two magnon scattering from the driven FMR mode to these extremely long wavelength EMSW modes had not been considered previously.

The above HFE linewidth results also lead to further realizations about the low field effective (LFE) linewidth response. The focus in Ref. 1 was on the EMSW modes that are slightly below the $\omega = ck_0/\sqrt{\varepsilon_r}$ light line dispersion, where ω is angular frequency, c is the light speed in vacuum, k_0 is the wave number (k) for pure electromagnetic waves, and ε_r is the relative dielectric constant. It is these low k and low ω below-the-light-line EMSW modes that give rise to the HFE linewidth response discussed in Ref. 1. The important point for the present work is that there are also low k and high ω EMSW modes that lie above the light line. Based on the high field effective linewidth results in Ref. 1, it is expected that both sets of EMSW modes, as well as the usual high k dipole exchange spin wave modes, can have a significant effect on the low field effective linewidth.

This paper reports on recent measurements of the LFE linewidth, $\Delta H_{\mathrm{eff}}^{(\mathrm{LF})}(H)$, and makes connections with the various classes of spin wave modes enumerated above. As with the connections in Ref. 1 between the HFE linewidth and the below-the-light-line EMSW modes, this connection is possible only because of (1) the extended capabilities for high accuracy effective linewidth measurements and (2) the refined understanding of the role of the EMSW and the dipole exchange branch spin waves in two magnon scattering.

Section II considers materials and the microwave measurement methods. Section III presents the experimental results. Section IV provides theoretical connections. Section IV A gives a brief overview of the spin wave band considerations relevant to the effective linewidth problem and Sec. IV B gives qualitative connections with the data from Sec. III. Sections IV C and IV D provide working equations for a theory of grain boundary scattering (GBS) and give quantitative connections with the low field effective linewidth data. Section V gives a summary and conclusion.

II. FERRITE MATERIALS AND MEASUREMENT METHODS

The samples and the details of the cavity measurement technique for the determination of effective linewidth are described in Ref. 1. This section provides a brief recap of the samples, the effective linewidth measurement, and analysis methods, and adds additional information that is needed to deal with the low field case.

The samples consist of nominal 2 mm diameter spheres fabricated from ultradense polycrystalline YIG and conventionally sintered Trans Tech G113 YIG starting materials. The UD sample is 99.9% dense or greater, relative to the theoretical YIG density. The CS sample is greater than 99% dense. High density gives low loss. The porosity contributions to the linewidth that often dominate the losses in many ferrites become small and even negligible.[6] Hence, many of the fine points related to intrinsic and two magnon scattering losses can be readily investigated. Another important consideration for the LFE linewidth will relate to grain size. The hipped UD sample has a nominal grain size of about 8 μm, while the CS G113 YIG samples have a grain size on the order of 20 μm.

The cavity is the same as in Ref. 1, a TE_{011} cylindrical cavity with a nominal center frequency of 10 GHz and nominal quality Q factor of 22 000. Based on the metrological ABA method given in Ref. 1, the cavity center frequency ω and quality factor Q were measured as a function of static external field H from a high field limit value of 7 kOe down to a low field limit of 1 kOe. As in Ref. 1, fields in the bulk manifold region of degenerate moderate k spin waves from 3 to 4.5 kOe were excluded. The high losses in the manifold region generally cause a severe degradation in the Q of the cavity and precision Q measurements are not possible. The low field limit of 1 kOe is set by the onset of sample demagnetization effects. The high field limit of 7 kOe was adequate to obtain the high field limit cavity frequency and Q values needed for the analysis.

For effective linewidth measurements in the low field regime, it is necessary to go beyond the approximate treatment for the high field ΔH_{eff} analysis in Ref. 1. At low field, one cannot assume *a priori* that the condition $\Delta H_{\mathrm{eff}} \ll H$ is valid. In addition, one cannot take the operational gyromagnetic ratio parameter that appears in the susceptibility expressions equal to the intrinsic gyromagnetic ratio. The equations below summarize the approach that gives exact expressions for ΔH_{eff} that are generally valid at any field, out of as well as in manifold.

One starts with the standard small signal microwave response of a spherical ferrite sample defined through the complex external susceptibility tensor $\boldsymbol{\chi}_e$. In the experiment, the cavity is used to measure the diagonal component χ_e of this tensor. It is convenient to rewrite χ_e explicitly in terms of the real part χ_e' and the negative imaginary part χ_e'', or as $\chi_e = \chi_e' - i\chi_e''$. The power absorbed by a ferrite sample scales with χ_e''. The full width at half maximum of the χ_e'' versus field profile corresponds to the usual FMR linewidth ΔH. As will be evident shortly, data for both χ_e' and χ_e'' are needed to obtain the effective linewidth ΔH_{eff} as a function of field.

One may obtain relatively simple expressions for χ_e from a torque equation of motion analysis with microwave loss introduced through a complex frequency approach or other means. For uniformly magnetized nonconducting spherical samples with a uniform linearly polarized micro-

Downloaded 14 Mar 2007 to 129.82.140.121. Redistribution subject to AIP license or copyright, see http://jap.aip.org/jap/copyright.jsp

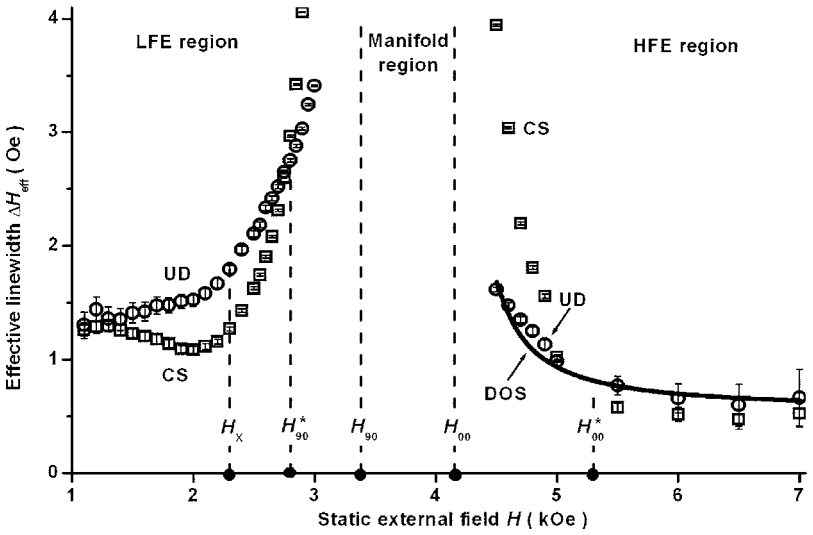

FIG. 1. Measured out-of-manifold effective linewidth ΔH_{eff} as a function of static external field H from 1 to 3 kOe and from 4.5 to 7 kOe for the nominal 2 mm diameter ultradense (UD) hipped and conventionally sintered (CS) YIG spheres at a nominal signal drive frequency of 10 GHz. The open circles and the open squares show the UD and the CS data, respectively. The error bars are shown for all data points. The vertical dashed lines indicate five important field reference points related to the spin wave band at H_X =2.3 kOe, H_{90}^*=2.8 kOe, H_{90}=3.38 kOe, H_{00} =4.15 kOe, and H_{00}^*=5.3 kOe. The low field effective (LFE) linewidth, manifold, and high field effective (HFE) linewidth regions are also labeled. The solid curve in the high field regime shows a best fit to the UD data based on $\Delta H_{\text{eff}}=A\cdot\text{DOS}+\Delta H_b$, where A is a constant scale factor, DOS denotes the density of states for the Larmor electromagnetic branch spin waves, and ΔH_b is a constant background linewidth parameter.

wave drive at frequency ω and a harmonic time dependence taken as $e^{+i\omega t}$, one may write the complex susceptibility as[4]

$$\chi_e = \chi_e' - i\chi_e'' = \frac{|\gamma|M_s(|\gamma|H + i\eta)}{(|\gamma|H + i\eta)^2 - \omega^2}, \tag{1}$$

where M_s denotes the magnetization of the sample and ω is the microwave drive frequency. The nominal saturation induction $4\pi M_s$ for YIG is 1750 G. The in phase χ_e' part of the response corresponds to dispersion. The out of phase χ_e'' part corresponds to loss.

In the past work, various ways have been used to extract $\Delta H_{\text{eff}}(H)$ from measurements of $\chi_e'(H)$ and $\chi_e''(H)$. A simple and direct method is used here. Based on Eq. (1) and the $\Delta H_{\text{eff}}=2\eta/|\gamma|$ connection, the effective linewidth can be obtained as

$$\Delta H_{\text{eff}} = \frac{2M_s H\chi_e''}{2H[(\chi_e')^2 + (\chi_e'')^2] - M_s\chi_e'}. \tag{2}$$

It is noteworthy that the working equation for ΔH_{eff} given in Eq. (2) does not involve the gyromagnetic ratio γ. In the present approach, a numerical value of γ is needed only for the cavity calibration needed for the determination of χ_e' and χ_e'' at a given field H. Calibration is considered below. Apart from this operation, therefore, γ does not play a crucial role in the analysis.

Based on standard microwave cavity perturbation theory methods, χ_e' and χ_e'' are related to the various cavity parameters through the equations $4\pi\chi_e'=-K(\omega-\omega_\infty)/\omega$ and $4\pi\chi_e''=K(1/Q-1/Q_\infty)/2$.[7] In the above, ω_∞ and Q_∞ correspond to the frequency and quality factor of the cavity, respectively, with the magnetic effects frozen out, so to speak. The K parameter is a cavity calibration factor that scales with the volume of the sample and depends on the nature of the electromagnetic mode in the cavity. These parameters are generally obtained from high field measurements with the sample in place and a high field extrapolation procedure. These calibration parameters are then taken to be applicable over the full out-of-manifold high and low field regimes. The above connections are valid as long as the sample loading of the cavity is relatively small and the changes in ω and Q, relative to ω_∞ and Q_∞, are not too large. Reference 1 contains complete details on the overall high field cavity calibration procedure. It is based on the fact that in the high field limit, χ_e' for the uniform mode is a function of H, M_s, ω, and γ only. No linewidth parameter is involved. The M_s value for YIG is known. One can see from the cavity response equations given above that the measured frequency ω should be a linear function of $4\pi\chi_e'(H,M_s,\omega,\gamma)$ with a slope of $-1/K$ and an intercept of ω_∞. The operational procedure was to (1) measure ω vs H in the high field regime, (2) plot the frequency as a function of $4\pi\chi_e'(H,M_s,\omega,\gamma)$, and (3) determine the γ value that renders the best linear function. The slope of this fit then gives K. In Ref. 1, the nominal free electron value of γ was used. The fitted γ values from the present procedure were slightly off the free electron value and consistent with known values for YIG.

Prior to the application of the full susceptibility analysis to obtain $\Delta H_{\text{eff}}(H)$ from the ω and Q data, an additional correction was applied to the measured Q values to account for the small but possibly significant frequency dependence of the nonmagnetic part of the quality factor. In the working equations given above, it is assumed that the Q change with field comes only from the magnetic losses. However, the change in the cavity frequency due to the change in χ_e' with field can also affect the Q through the frequency dependence of the conductivity losses in the cavity walls. The nonmagnetic Q of a microwave cavity generally scales with the inverse of the electromagnetic skin depth of the metal that makes up the cavity, and this skin depth, in turn, scales with $1/\sqrt{\omega}$.[8] If the frequency changes are small, this means that the frequency shift Q correction is given as $\delta Q=Q_\infty(\omega-\omega_\infty)/2\omega$ and the $4\pi\chi_e''Q$ connection changes to $4\pi\chi_e''=K[1/(Q-\delta Q)-1/Q_\infty]/2$. One uses δQ, as obtained directly from the data, to back correct from the measured Q and f at a given field to the value without the eddy current shift of the nonmagnetic Q from Q_∞. For the present low loss samples, this correction, along with the changes in the ΔH_{eff} calculation procedure from that used in Ref. 1, amount to a change in the LFE linewidth by 10% or less.

Downloaded 14 Mar 2007 to 129.82.140.121. Redistribution subject to AIP license or copyright, see http://jap.aip.org/jap/copyright.jsp

III. EFFECTIVE LINEWIDTH EXPERIMENTAL RESULTS

Figure 1 shows representative measurement results on the nominal 10 GHz out-of-manifold effective linewidth at both low and high fields. The open circles and squares show the data for the UD and the CS YIG samples, as indicated. The graph shows HFE linewidth data for fields from about 4.5 to 7 kOe and LFE linewidth data for fields from about 1 to 3 kOe. No data are shown in the high loss manifold region delineated by the vertical dashed lines at $H=3.3$ kOe (H_{90}) and $H=4.15$ kOe (H_{00}), or below 1 kOe in the region where spherical samples start to demagnetize. The vertical dashed lines labeled H_{00}^{*} and H_{90}^{*} are the shifted H_{00} and H_{90} field points which are shifted due to local pore demagnetizing fields.[5] The vertical dashed H_X reference line marks a transition field for EMSW dispersion properties. These field designations will be important for the discussion of Sec. IV. The solid curve overlaid to the data in the HFE region with the DOS label shows a fit to the UD data as described in the caption. These fit results will be considered shortly.

What do these data show? Consider the high field (HFE) region first. The high field data for both samples show a gradual decrease in effective linewidth as the field is increased. For fields above the H_{00}^{*} point, both sets of data also closely follow to the scaled DOS curve. For fields below the H_{00}^{*} point, however, the HFE linewidth data points for the CS sample break from the UD data and the computed DOS curve. This break is related to pore-demagnetizing field and pseudo-in-manifold two magnon scattering effects.[9] Such pseudo-in-manifold two magnon scattering will also be a consideration for the LFE linewidth results.

For the low field effective linewidth results, there are two general observations and several important details. The first general observation is that the LFE linewidths in Fig. 1 are generally larger than the HFE linewidth values. The second is that the relative UD and CS ΔH_{eff} values are now reversed, as compared to the high field response. The LFE linewidths for the UD sample are generally larger than those for the CS sample.

With regard to the details, the most obvious point is in the change in the ΔH_{eff} vs H responses for both samples close to the H_X point. Above $H=H_X$ but below $H=H_{90}^{*}$, both linewidths increase rapidly with field but the change for the CS sample is more rapid than that for the UD sample. The CS linewidths start out smaller but increase more rapidly than the UD as one moves from the H_X point to larger fields. There is also an apparent crossover of the data for the two samples at a field close to $H=H_{90}^{*}$. Finally, as one moves below $H=H_X$, the ΔH_{eff} for the UD sample continues to decreases, albeit with a weaker response, while the CS data show an increase.

IV. TWO MAGNON SCATTERING AND THE EFFECTIVE LINEWIDTH

A. Spin wave band considerations

In order to analyze and understand the data presented above, it is necessary to consider the multiband spin wave picture from Ref. 1 for high fields and extend this picture to the low field regime as well. The spin wave bands that result from a full solution of Maxwell's equations and the linearized torque equation of magnetization motion for plane wave spin waves in an infinite insulating medium were presented in the seminal text *Microwave Ferrites and Ferrimagnetics* by Lax and Button.[10] One may also write the analytical spin wave band response in the form of a governing equation,

$$H_i = 4\pi M_s\left[\frac{k^2(1+\cos^2\theta_k)}{2(k^2-k_0^2)}-1\right] - Dk^2 \pm \sqrt{\frac{\omega_k^2}{\gamma^2}+\frac{(4\pi M_s)^2k^4\sin^4\theta_k}{4(k^2-k_0^2)^2}} = H-\frac{4\pi M_s}{3}. \tag{3}$$

In the above, H_i denotes the static internal field, θ_k denotes the spin wave polar propagation angle relative to the static field direction, ω_k is the spin wave frequency, and D is an exchange parameter. All other parameters are the same as given previously. Equation (3) applies to any material with a homogeneous internal field. The last term, $H-4\pi M_s/3$, is included only to make a specific connection with the external field H for spherical samples. When one chooses the "+" in front of the square root term, one obtains the dispersion branches for modes with a Larmor (L) sense of precession. Choice of the "−" gives the anti-Larmor (A) precession branches. Recall that $k_0=\sqrt{\varepsilon_r}\omega/c$ denotes the wave number for pure electromagnetic waves. For YIG materials, one has $\varepsilon_r\approx 10$ and $D\approx 5.2\times 10^{-9}$ Oe cm^2.

One can view Eq. (3) in several ways. The traditional way is to consider the field H (or H_i) as fixed and examine the various $\omega_k(k)$ dispersion bands that are formed as θ_k is scanned from zero to $\pi/2$. One can then make a frequency cut at some selected driving frequency of interest, such as the signal frequency ω in the effective linewidth experiment, for example, and obtain a determination of those modes that are degenerate with the drive signal frequency ω. Alternatively, one can arrive at this same determination of degenerate modes by considering a fixed spin wave frequency at $\omega_k=\omega$ and then solving for the dispersion bands in k for $0<\theta_k<\pi/2$ as a function of H. Both approaches will be used below.

Figures 2 and 3 show spin wave band diagrams that elucidate the manner in which these degenerate spin wave mode populations change with field. All diagrams were obtained for YIG parameters. The graphs in Fig. 2 show traditional plots of spin wave frequency ω_k vs k for two specific fields, as indicated. The dashed line horizontal frequency cuts at $\omega_k/2\pi=10$ GHz indicate the nominal signal frequency for the current effective linewidth measurements. The single graph in Fig. 3 shows the corresponding plot of wave number k versus the external field H for a spherical sample with the frequency $\omega_k/2\pi$ set to 10 GHz. The field scale is the same as used for Fig. 1. The bands evident in these graphs are formed from dispersion branches that range from wave vectors that are parallel to the static field ($\theta_k=0$) to wave vectors that are perpendicular to the field ($\theta_k=\pi/2$). The bands are labeled as EML-HI, EMA, EML-LO,

Downloaded 14 Mar 2007 to 129.82.140.121. Redistribution subject to AIP license or copyright, see http://jap.aip.org/jap/copyright.jsp

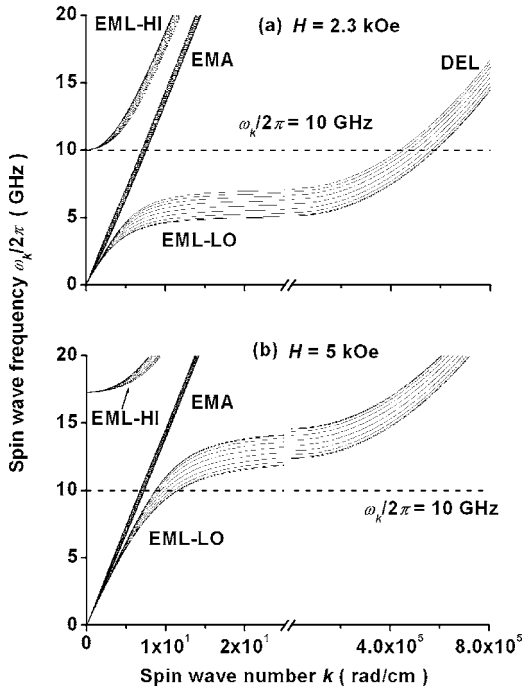

FIG. 2. Graphs (a) and (b) show full infinite medium spin wave band diagrams of the spin wave frequency $\omega_k/2\pi$ as a function of the positive real wave number k for YIG sphere parameters and external static fields of 2.3 and 5 kOe, respectively. The bands of contours correspond to propagation angles (θ_k), relative to the static field, from 0° to 90°. The curves group into three bands, the nearly straight line light line EMA band, the hybrid below-the-light-line EML-LO (low k) to DEL (high k) band, and the above-the-light-line EML-HI band. The graphs also show dashed reference lines at $\omega_k/2\pi=10$ GHz.

and DEL in all the graphs. The EML-LO and DEL labels actually correspond to the same band for low and high k ranges, as indicated.

It is important to take note of the band label nomenclature in the figures. An important line of reference is the narrow straight EMA band in the Fig. 2 graphs and the corresponding nearly horizontal band in Fig. 3. These narrow bands correspond to the light line at $\omega_k=ck/\sqrt{\varepsilon_r}$ in the nonmagnetic limit. The EML-HI labels identify the above-the-light-line band just above this light line band in the Fig. 2 graphs. The EML-LO labels identify the below-the-light-line band in these graphs. At high k, the EML-HI band converges with the light line, while the EMA-LO band moves farther and farther away and finally evolves into the DEL band. The DEL band is so labeled to denote the dipole-exchange (DE) and Larmor (L) nature of the high k far-from-the-light-line response. The "L" in EML also denotes the precession response as Larmor. The "A" in EMA denotes the anti-Larmor precession associated with the light line band.

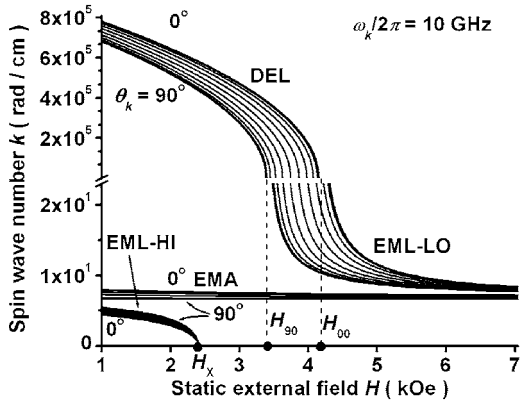

FIG. 3. Infinite medium spin wave band diagram of the positive real spin wave wave number k as a function of the static external field H for YIG sphere parameters and a spin wave frequency $\omega_k/2\pi=10$ GHz. The bands of contours correspond to propagation angles (θ_k) of 0° to 90°, relative to the static field, as indicated. The curves group into three bands, the nearly flat EMA band, the hybrid DEL (high k and low field) to EML-LO (low k and high field) band, and the low k and low field ($H<H_X$) EML-HI band. The H_X, H_{90}, and H_{00} labels indicate, respectively, the fields at which the EML band limit frequency at $k=0$ sits at 10 GHz and the points in field at which the $\theta_k=90°$ and $\theta_k=0$ low k limit frequencies for the DEL band sit at 10 GHz.

The notation here follows that used in Ref. 1, except for the additional "HI" and the "LO" designations that are now invoked to designate the above-the-light-line and the below-the-light-line EMSW bands in Fig. 2. In Ref. 1, only the EML-LO band (as now labeled) was important for the high field effective linewidth. For the low field effective linewidth, it is the EML-HI and DEL bands that play important roles. Note that the different bands flip positions relative to the EMA light line band in going from Fig. 2 to Fig. 3.

The advantage of the Fig. 2 format is that one can see the full spin wave band scheme in reference to the specific slice of modes that are degenerate with the 10 GHz drive frequency for given field values. The $H=H_X=2.3$ kOe field point for (a) demonstrates the two magnon scattering connections that are relevant to the low field effective linewidth. This is also the particular value for which the EML-HI band converges to the $\omega_k/2\pi=10$ GHz reference line at $k=0$. The $H=5$ kOe value for (b) was chosen to show the position of the spin wave bands that are relevant to the high field effective linewidth.

The advantage of the Fig. 3 format is that one can see directly the manner in which the wave numbers for the modes that are degenerate with the 10 GHz drive frequency change with field. The labels H_X, H_{90}, and H_{00} along the field axis show, respectively, the point in field at which the above-the-light-line EMSW band limit frequency at $k=0$ sits at 10 GHz, and the points in field at which the $\theta_k=90°$ and $\theta_k=0$ low k limit frequencies for the DEL band also sit at 10 GHz. From the dispersion bands in Fig. 3 and the H_X, H_{90}, and H_{00} labels, one can now see why these points in field are identified in Fig. 1.

B. Qualitative two magnon scattering connections

1. Recap of high field effective linewidth origins

As a starting point for the discussion of the low field data, spin waves, and two magnon scattering, it is useful to begin with a brief recap of the high field results from Ref. 1. Turn, therefore, to Fig. 2(b) and the high field regime in Fig. 3. From Fig. 2(b), one sees that for high fields, the main DEL band is shifted well above the $\omega_k/2\pi=10$ GHz reference line. From Fig. 3, one sees that the available degenerate modes in the high field regime all belong to the EML-LO

Downloaded 14 Mar 2007 to 129.82.140.121. Redistribution subject to AIP license or copyright, see http://jap.aip.org/jap/copyright.jsp

band or to the EMA band. It is the EML-LO modes that dominate the effective linewidth in the high field regime.

There are three main points of note for the high field ΔH_{eff} data. First, the decrease in the HFE linewidth with increasing field for the UD and CS materials for the $H > H_{00}^{*}$ field regime in Fig. 1 is due to the decrease in the density of states for the modes in this EML-LO band. As one moves to higher and higher fields, the 10 GHz cut across the EML-LO band becomes smaller and smaller. The solid curve in Fig. 1 represents a best fit to a function of the form $\Delta H_{\text{eff}} = A \cdot \text{DOS} + \Delta H_b$, where A is a constant scale factor equal to 7540 Oe cm^3 MHz, DOS denotes the density of states for the Larmor electromagnetic branch spin waves, and ΔH_b is a constant background linewidth parameter set to 0.35 Oe. The good matchup of the UD data with the solid curve for $H > H_{00}^{*}$ is convincing evidence that the EML-LO band two magnon scattering is responsible for the HFE linewidth field response. The numerical scale factor A will play a role in the theoretical analysis of the low field ΔH_{eff} results. This scattering to the extremely low k EML-LO band of modes is relatively weak and the effective linewidths are only slightly larger than the background linewidth of 0.35 Oe.

The second point is that the high field ΔH_{eff} extrapolates to near intrinsic linewidth values in the extreme high field limit. The fitted ΔH_b value of 0.35 Oe is close to established values of the 10 GHz linewidth in single crystal YIG.[11] These so-called intrinsic linewidths in this range for single crystal YIG are typically associated with various magnon phonon processes other than two magnon scattering. This also means that the anti-Larmor EMA band spin waves make essentially no contribution to the HFE linewidth. Because the EMA band is more or less flat as a function of field, as in Fig. 3, this implies that the EMA band is not important for the LFE linewidth as well.

The third important aspect of the high field response concerns the more rapid rise in the high field ΔH_{eff} for the CS sample as the field drops below H_{00}^{*}. This effect is due to differences in microstructure and, in particular, the effect of pores. The maximum spherical pore demagnetizing field in the direction opposite to the applied field, just at the top and bottom of the pore, is about $8\pi M_s/3$. This is precisely the separation of the H_{00}^{*} point from the H_{00} (no asterisk) point at the high field edge of the manifold region. As H drops below H_{00}^{*}, there are regions in the CS sample that correspond to a local in-manifold bias field and there is a corresponding increase in the effective linewidth. There is a counterpart pseudo-manifold effect at low field that involves H_{90} and H_{90}^{*}. This effect will be considered shortly.

2. Low field effective linewidth origins

Now consider the low field spin wave band picture in Fig. 2(a) and the low field degenerate mode picture in Fig. 3. The degenerate mode situation for the low field regime is quite different from that at high field. There are three specific changes of note: First, the previously degenerate EML-LO modes are all well below the $\omega_k/2\pi = 10$ GHz frequency cut, as in Fig. 2(a). From the Fig. 3 display, one sees that the EML-LO modes that dominate the two magnon scattering contribution to the HFE linewidth are completely out of the picture for the LFE linewidth.

Second, the high k DEL modes that were previously found at frequencies well above the signal frequency now actually cross the 10 GHz cut, as in Fig. 2(a). From the Fig. 3 display, one sees that there are degenerate high k DEL modes over the entire low field regime. This means that one can have scattering to these high k DEL modes over the entire low field regime. However, these high k modes have very short wavelengths in the submicron range. For a significant contribution to ΔH_{eff}, the scattering to such modes will invoke considerations of grain boundaries and not simply the micron sized grains of the polycrystal. On the other hand, the large density of states that one finds at high k will promote strong scattering, even if the actual coupling is small. These points will be considered in more detail shortly.

Third, for the particular choice of field at $H = H_X$ for graph (a) of Fig. 2, one can see that the EML-HI band is touching the 10 GHz line just at $k = 0$. If the field is dropped further, to some value below H_X, the EML-HI band will drop even more in frequency and the 10 GHz cut will then include modes for this band. Figure 3 shows this explicitly. The changes in the low field ΔH_{eff} versus field response at $H = H_X$ in Fig. 1 for both the UD and the CS samples may be attributed to the vanishing DOS component at 10 GHz for the EML-HI band for $H > H_X$ and the appearance of an EML-HI DOS component for $H < H_X$. Any change in the actual scattering, of course, will involve modes with low wave numbers and extremely large wavelengths. These are the same type of modes that are now known to play an important role in the high field effective linewidth, except that the EML-HI modes now replace the EML-LO modes and there is now the additional effect of a field cut-off effect for $H > H_X$.

Turn now to specific mode connections from Figs. 2(a) and 3 to the low field effective linewidth. First consider the two general points from Sec. III the larger ΔH_{eff} at low field, relative to high field, and the interchange in the relative values of the effective linewidths for the UD and CS samples. One can now see that the basis for a larger ΔH_{eff} in the low field regime, relative to high field, is that there are simply more degenerate modes. In the low field regime, one always has degenerate DEL band modes. The high k nature of these modes generally means a larger density of states.

The high k DEL mode scattering is also the key to the interchange of the relative ΔH_{eff} values, with those for the UD sample now greater than those for the CS samples. One can see from Fig. 3 that the degenerate DEL modes have k values in the 10^5 rad/cm range, with corresponding wavelengths well into the submicron range. As already noted, scattering to such short wavelength modes will be connected more closely with grain boundaries, rather than with grains and pores, and this will favor the relatively smaller grain UD sample. The smaller grain size for the UD sample means a larger net grain boundary area and more scattering, relative to the high k scattering for the CS sample. Simple geometric arguments give a grain boundary area that scales with the grain size a as $1/a$. This means that the UD sample, with

Downloaded 14 Mar 2007 to 129.82.140.121. Redistribution subject to AIP license or copyright, see http://jap.aip.org/jap/copyright.jsp

$a \approx 8$ μm, will have a little more than double the grain boundary area of the CS sample with $a \approx 20$ μm. It is reasonable, therefore, to see a higher ΔH_{eff} for the UD sample in the low field regime.

The details of the low field ΔH_{eff} vs H dependences demonstrated in Sec. III an also be placed into a clear spin wave perspective, based on the diagrams in Figs. 2 and 3. The role of the H_X field point is clear from both figures. The changes in the ΔH_{eff} vs H responses for both data sets at $H=H_X$ are clearly related to the onset of mode degeneracy for the EML-HI modes at this field. The more rapid rise in the ΔH_{eff} for the CS sample, relative to that for the UD sample, for $H>H_X$ must be related to the different interplay between the coupling and the density of states for these different microstructures.

The apparent crossover in the low field ΔH_{eff} at $H=H_{90}^{*}$ and the larger CS ΔH_{eff} as one moves into the low field pseudo-manifold region for $H>H_{90}^{*}$ are consistent with the similar effect in the high field regime for $H<H_{00}^{*}$. Here, however, one must consider the maximum value of the pore demagnetizing field that is parallel to the static field. For a spherical pore, this maximum demagnetizing field occurs at the sides of the pore and is equal to $4\pi M_s/3$. The field point at $H=H_{90}^{*}$ is shifted down from H_{90} by this amount. A close examination of the low field data in Fig. 1 shows, moreover, that the UD and the CS data points appear to cross at precisely this point in field. The rise in ΔH_{eff} for both samples as the field is increased is already quite rapid in this local region, and it is difficult to tell if there is an actual increase in the slope of the response as one would expect from an onset of pseudo-in-manifold scattering for $H>H_{90}^{*}$.

Finally, there are the quite different ΔH_{eff} responses for $H<H_X$. This is the region where the EML-HI modes come into play. Given the fact that the EML-LO modes give rise to the same ΔH_{eff} vs H responses for $H>H_{00}^{*}$ in the high field regime, while the EML-HI modes give rise to different responses for the UD and the CS samples in the low field regime with $H<H_X$, one can surmise that some different aspects of the low k scattering must be coming into play. It may be noteworthy that the two linewidths are roughly equal for an external field slightly above 1 kOe. This is about the point at which the spherical YIG samples will start to demagnetize. Demagnetization will tend to average out polarization effects.

C. Grain boundary scattering and quantitative connections with low field effective linewidth

This section considers a theory of GBS and connections with the present data. The full theory will be published separately. As already noted, the relevant k values are in the 10^5 rad/cm range and one needs submicron inhomogeneities to provide a source for the two magnon coupling. The grains in the UD and CS YIG materials are in the 5–20 μm range. The main candidate for high k scattering, therefore, is in grain boundaries and related defects.

Formally, one may write the two magnon relaxation rate η_{TM} as an integral over the available $\mathbf{k}$ states at $\omega_k=\omega$ that takes into account the density of states and the coupling to the modes. One then obtains the effective linewidth as $\Delta H_{\text{eff}}=2\eta_{\text{TM}}/|\gamma|$. The η_{TM} integral can be written in the form

$$\eta_{\text{TM}} = \frac{\omega_M^2}{4\pi^2}\int d\mathbf{k} C(\mathbf{k})\Lambda(\omega,\mathbf{k})\delta(\omega_k-\omega). \tag{4}$$

The ω_M parameter is equal to $|\gamma|4\pi M_s$. The $\delta(\omega_k-\omega)$ function serves to constrain the considered spin wave modes to those for the particular ω_k band of interest and those particular modes that are degenerate with the signal frequency. The delta function integral alone corresponds to the density of states. The coupling factor $C(\mathbf{k})$ determines the strength of the coupling between the uniform mode and the spin waves due to the grain boundaries. The mode polarization factor $\Lambda(\omega,\mathbf{k})$ takes the ellipticity of the spin wave modes into account. The paragraphs below outline the essential physics of the low field scattering, provide recipes for actual evaluations, and present fits to the data based on the theory.

Consider first the basic variation in the DOS for the degenerate modes as a function of field. Density of states is a basic concept in solid state physics. The starting assumption is that the allowed plane wave modes are uniformly distributed in $\mathbf{k}$ space. It is then a matter of geometry and the details of the given dispersion connections to obtain the number of modes $dn(\omega_k)$ per unit volume for a given slice of frequency space from ω_k to $\omega_k+d\omega_k$. The relation $dn(\omega_k)=g(\omega_k)d\omega_k$ then serves as a definition of a DOS function $g(\omega_k)$. For the multiband spin wave situation at hand, $g(\omega_k)$ becomes the field dependent $g(\omega_k,H)$ DOS function for the total density of states for all of the modes degenerate with a given ω_k. This is because the k solutions in Eq. (3) also depend on H. For a given band of interest, one obtains a working equation of the form,

$$g(\omega,H) = \frac{1}{2\pi^2}\int_0^{\pi/2} k^2(\omega,\theta_k,H)\frac{\partial k(\omega,\theta_k,H)}{\partial\omega}\sin\theta_k d\theta_k. \tag{5}$$

The density of states weighting function is embodied in the integral of Eq. (4) through the $\delta(\omega_k-\omega)$ constraint. The density of states plays an important role in two magnon scattering.

Note that the integral in Eq. (5) is over the spin wave propagation angle θ_k only. This corresponds to a vertical line cut in Fig. 3 at a fixed field across the available modes. For the two magnon scattering problem, one solves Eq. (3) for the positive real $k(\omega_k,\theta_k,H)$ roots for the DEL, EML-LO, and EML-HI bands, obtains the derivative functions needed for Eq. (5), and then evaluates the integrals for $\omega_k=\omega$. These evaluations are done numerically to obtain $g(\omega,H)$ as a function of H. The dispersion relation in Eq. (3) connects k to θ_k, and one can reduce the k-space integral to the form given above. For specific ω and H values, $g(\omega,H)$ can be easily evaluated by numerical methods for any known dispersion connection.

Figure 4 shows calculated density of states curves for $g(\omega,H)$ as a function of the static external field H at $\omega/2\pi=10$ GHz for the DEL, DEL-LO, and EML-HI bands, as indicated. The curves were obtained for YIG parameters. Curves for the EMA band are excluded. The DOS curves in

Downloaded 14 Mar 2007 to 129.82.140.121. Redistribution subject to AIP license or copyright, see http://jap.aip.org/jap/copyright.jsp

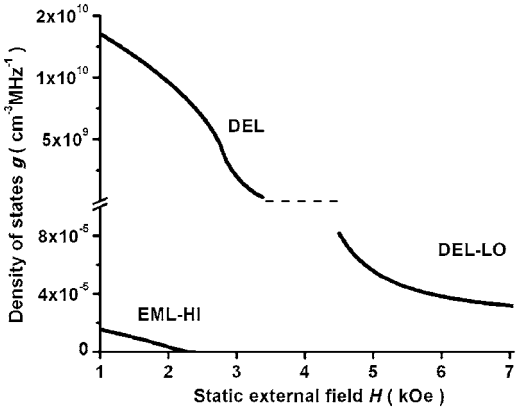

FIG. 4. Integrated 10 GHz density of degenerate states g as a function of static external field H for the DEL, EML-HI, and EML-LO spin wave bands, as indicated. The curves were obtained for YIG parameters and sphere shaped samples.

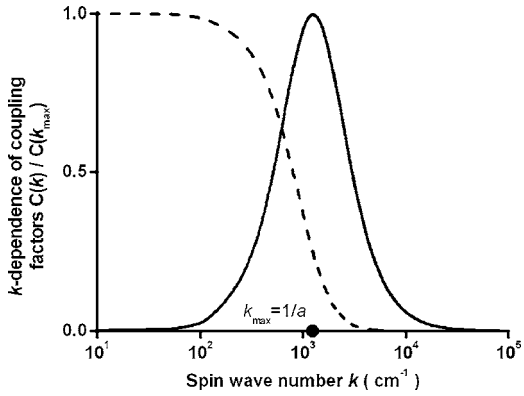

FIG. 5. The solid curve shows the scaled grain boundary scattering coupling factor $C(k)/C(k_{\max})$ as a function of wave number k, where $k_{\max}=1/a$ marks the peak position. Here, a is the average grain size. The dashed curve shows the scaled coupling factor for isotropic grain scattering due to anisotropy. The curves are for $a=8$ μm.

Fig. 4 quantify many of the basic features mentioned in the previous sections. For the low field DEL band of primary interest here, the $g(\omega,H)$ values are rather large, on the order of $10^{10}-10^{11}$ cm^{-3} MHz^{-1}. These large values are due to the large wave numbers for the dipole exchange spin waves, on the order of 10^5 rad/cm, and the corresponding large volume of k space. The density of states remains relatively high as one moves to the bulk manifold region and the horizontal dashed transition line from DEL to EML-LO modes in Fig. 3. This is because high k as well as low k spin waves are available. For the EML-LO band that is present only at high field, the wave numbers are small and $g(\omega,H)$ is also small, typically on the order of 10^{-5} cm^{-3} MHz^{-1}. This matches the situation considered in Ref. 1. The EML-HI band only comes in for fields below $H=H_X$. The density of states for these modes is even smaller, mainly due to the extremely low values of k for this above-the-light-line spin wave band.

Turn now to the coupling and polarization functions in Eq. (4). The GBS theory is based on a simple model of partial pinning at the grain boundaries and the assumption of random grains with an average grain size a. Fourier transforms, correlations, and statistical averaging are used to obtain a $C(\mathbf{k})$ coupling factor that may be written as

$$C(\mathbf{k}) = C(k) = \frac{6\pi k^2 \ell_{\rm gb}^2 a^3}{(1+k^2a^2)^2}, \tag{6}$$

where $\ell_{\rm gb}$ is an effective grain boundary thickness parameter. Much of the formal analysis follows from the approach of Schlömann for the isotropic anisotropy scattering.[12,13] That is, there is no dependence on the direction of $\mathbf{k}$.

The $\ell_{\rm gb}$ parameter derives from a surface or interface anisotropy energy density at the grain boundary and is essentially the ratio of this energy density to the magnetostatic self-energy $2\pi M_s^2$.[14] This interaction serves to provide a partial pinning of dynamic magnetization at the grain boundary. As shown below, if the measured LFE linewidths are taken to originate from a GBS process, one obtains $\ell_{\rm gb}$ values in the nanometer range.[15] These are reasonable values for grain boundaries in dense ferrite materials. The corresponding surface anisotropy energies are on the 0.1 erg/cm^2 range. This is also reasonable for a surface or interface anisotropy. As one might expect, the fact that $\ell_{\rm gb}$ is fairly small means that the coupling factor is also small. The sizable effective linewidths due to low field grain boundary scattering derive from the high density of states for the DEL modes in the low field regime. Note that this type of GBS model is not valid for porous materials. Scattering based on an interface anisotropy is not valid when there are voids between the grains.

Figure 5 shows a normalized plot of $C(k)/C_{\max}(k)$ from Eq. (6) as a function of k. The grain size a was set at 8 μm, the nominal grain size for the UD YIG material. Note that the horizontal k scale is logarithmic. The coupling factor is a maximum at $k_{\max}=1/a$ and it exhibits a rather broad and nonsymmetric-peak-type response. On a linear k scale, the half maximum points in k occur at $0.414/a$ and $2.414/a$, for a half width of $2/a$. The dashed curve in Fig. 5 shows the coupling factor that one would expect for grain scattering. The grain scattering coupling is essentially constant for $k<k_{\max}$ and falls to zero fairly rapidly for $k>k_{\max}$. One can see that grain boundary scattering is much different from grain scattering.

As noted, the remaining $\Lambda(\omega,\mathbf{k})$ factor in Eq. (4) is related to the change in the spin wave ellipticity as one ranges over the allowed θ_k values for the band. The $\Lambda(\omega,\mathbf{k})$ function may be written as

$$\Lambda(\omega,\mathbf{k}) = \frac{1}{2\omega}\left[|\gamma|H_i + |\gamma|Dk^2 + \omega + \frac{\omega_M \sin^2\theta_k}{2}\right]. \tag{7}$$

At $\omega/2\pi=10$ GHz and $H=2$ kOe for sphere shaped YIG samples, $\Lambda(\omega,\mathbf{k})$ will range from about 0.68 at $\theta_k=0$ to 0.82 at $\theta_k=90°$. The change with field from $H=1$ kOe to $H=2$ kOe amounts to about 20%. This causes a small ellipticity contribution to the field dependence of $\eta_{\rm TM}$ in Eq. (4).

Figure 6 shows results on the computed GBS contribution to the low field effective linewidth as a function of field based on the prescription given above. The solid circle data points show the low field $\Delta H_{\rm eff}$ data for the UD YIG sample from Fig. 3. The graph extends from the low field 1 kOe limit used for Fig. 3 up to the edge of the manifold region at H_{90}. The calculations include only the GBS scattering for the DEL band of modes. The effective grain boundary thickness

Downloaded 14 Mar 2007 to 129.82.140.121. Redistribution subject to AIP license or copyright, see http://jap.aip.org/jap/copyright.jsp

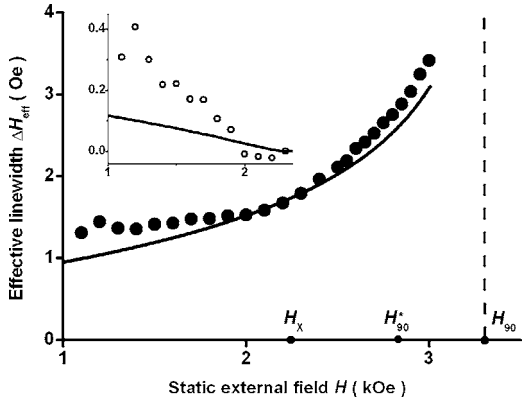

FIG. 6. Effective linewidth ΔH_{eff} vs static external field H for a spherical yttrium iron garnet (YIG) sample. In the main graph, the solid circles show the data from Fig. 1 for the ultradense (UD) YIG sample and the solid curve shows the computed linewidth due to grain boundary scattering. The dashed vertical line indicates the low field edge of the low wave number DEL spin wave manifold. The H_X and the H_{00} field points are the same as in Fig. 1. The open circles in the inset show the difference values for the data in the main graph for $H<H_X$, relative to the solid line. The solid curve shows the expected contribution to the LFE linewidth from EML-HI scattering, based on the scaling from the high field results.

parameter ℓ_{gb} was set at 9.5 nm and the average grain size a was set at the nominal value of 8 μm for the UD sample. This particular choice for ℓ_{gb} was made by fine tuning the calculated curve to give the match to the data as shown. As noted above, an ℓ_{gb} value of 10 nm or so is reasonable for dense polycrystalline ferrites. The $|\gamma|$ and $4\pi M_s$ values were the same as given above for YIG. The curve includes no provision for an offset residual linewidth.

The open circle points in the inset graph in Fig. 6 show the difference between the measured linewidth results for $H<H_X$ and the GBS theoretical values. The solid curve in the inset is based on the DOS for the EML-HI band of modes and the numerical scaling factor A obtained from the fit of the EML-LO DOS response to the HFE data. The curve shows only the expected two magnon scattering linewidth for the EML-HI modes based on this scaling. No other contributions are included.

One can see from the main graph in Fig. 6 that the GBS mechanism gives a reasonable semiquantitative match to the LFE linewidth data over the applicable high k scattering region in the field region between H_X and H_{00}. The term "semiquantitative" is used because it was not possible to obtain a good fit when a background level linewidth was added to the GBS response. This indicates that further refinements of the GBS model are needed to include a grain size distribution and possibly other factors. In spite of these problems, the matchup in the overall linewidth values for $H_X<H<H_{00}$ and the reasonable values of the GBS model parameters support the thesis of two magnon scattering from the driven uniform mode to DEL band spin waves as the origin of this low field response.

D. The LFE linewidth below $H=H_X$ and EML-HI scattering

As already noted in the previous sections, the upward deviation of the data from the theoretical curve for $H<H_X$ can be attributed to the appearance of additional low k scattering to the EML-HI modes at low field. The data in Fig. 6 show that the amount of deviation in the measured ΔH_{eff} from the GBS curve increases from near zero to more than several tenths of an oersted as H drops below H_X. At first glance, one might take this full deviation as a measure of the change in the density of states for the EML-HI modes with field and solid evidence for a significant two magnon EML-HI scattering effect.

The results in the inset of Fig. 6, however, indicate that this may not be the whole story. The solid curve shown in the inset shows the expected amount of low field effective linewidth from scattering to the EML-HI modes based on the scale parameter A obtained from the high field fit shown in Fig. 1. One can see that the predicted increase in the two magnon EML-HI scattering based effective linewidth falls well short of the observed increase. As a caveat, one also has to realize that all of these linewidth values are extremely small, on the order of or smaller than even the expected intrinsic linewidths.

One possible explanation for this discrepancy is that a different DOS scaling parameter for the low field EML-HI scattering is needed, relative to the high field EML-LO A value. At the few tenths of an oersted level, the differences in the ellipticity for these low field and high field spin wave branches, among other things, could be substantial and require a different scaling.

There are other options as well. It was more than four decades ago that Hartwig *et al.*[16] noted a peculiar subthreshold effect for parallel pumping in YIG single crystal spheres. These authors observed a rapid increase in the longitudinal microwave permeability loss component just as the applied field drops below the H_X point. Follow-up theory by Joseph and Schlömann[17] gave reasonable support to the presence of a subthreshold longitudinal susceptibility loss component that comes into play due to the in-manifold low k spin waves at one-half the pump frequency, just as the field drops below H_X. If there is indeed such a subthreshold longitudinal loss component, there could also be a subthreshold transverse loss component. Further work on the LFE linewidth for large single crystal YIG spheres is needed to address these issues.

V. SUMMARY

The above sections have described a refined method for precision measurement of the out-of-manifold effective linewidth in bulk ferrite materials. Specific measurements are reported for two materials, ultradense polycrystalline yttrium iron garnet produced by hot isostatic pressing and conventional sintered YIG with a moderate porosity. The data and corresponding analysis give insight into the origins of microwave loss in ferrites at low as well as high fields. In parallel with the high field results in Ref. 1, the low field effective linewidth is shown to be due to scattering to electromagnetic spin waves and pseudo-in-manifold spin waves.

The LFE linewidth, however, is attributed to two extra sources of scattering. From the low field edge of the low k spin wave band down to a cut-off field H_X point for the appearance of low wave number EML-HI modes, the effec-

Downloaded 14 Mar 2007 to 129.82.140.121. Redistribution subject to AIP license or copyright, see http://jap.aip.org/jap/copyright.jsp

tive linewidth is consistent with a grain boundary scattering model that couples the uniform mode to very high k DEL spin waves. Fits based on a theory of grain boundary scattering show semiquantitative agreement with the data. Problems for a complete quantitative agreement remain in that the match to the data is not possible if one includes any reasonable level of background intrinsic loss in the model.

For fields below H_X, the data show clear evidence for an additional low k two magnon scattering contribution from the EML-HI modes. However, a computed EML-HI two magnon scattering response, with a calibration based on the high field results, falls somewhat short of the measured values. Possible problems here include calibration issues and the possibility of an additional subthreshold nonlinear loss effect.

ACKNOWLEDGMENTS

This work was supported in part by the United States Office of Naval Research, Grant No. N00014-06-1-0889, and the U.S. Army Research Office, Grant No. W911NF-04-1-0247. The ultradense hipped YIG materials were prepared by G. M. Argentina and Dr. H. J. Van Hook. The conventionally sintered G113 YIG materials were provided by Trans Tech, Inc., Adamstown, Maryland. Kevin R. Smith and Dr. Steven N. Stitzer are gratefully acknowledged for careful reviews of the paper.

[1] N. Mo, Y. Song, and C. E. Patton, J. Appl. Phys. **97**, 093901 (2005).
[2] C. E. Patton, J. Appl. Phys. **41**, 1355 (1970).
[3] T. Kohane and E. Schlömann, J. Appl. Phys. **39**, 720 (1968).
[4] C. E. Patton, Phys. Rev. **179**, 352 (1969).
[5] Q. H. F. Vrehen, J. Appl. Phys. **40**, 1849 (1969).
[6] A. V. Nazarov, D. Ménard, J. J. Green, and C. E. Patton, J. Appl. Phys. **95**, 7227 (2003).
[7] J. J. Green and T. Kohane, Semicond. Prod. Solid State Technol. **7**, 46 (1964).
[8] J. D. Jackson, *Classical Electrodynamics* (Wiley, New York, 1998).
[9] U. Hoeppe, International Conference on Ferrites ICF9, San Francisco, August 2004 (unpublished).
[10] B. Lax and K. J. Button, *Microwave Ferrites and Ferrimagnetics* (McGraw-Hill, New York, 1962).
[11] M. Sparks, *Ferromagnetic-Relaxation Theory* (McGraw-Hill, New York, 1964).
[12] E. Schlömann, IEEE Trans. Magn. **1**, 75 (1970).
[13] E. Schlömann, Phys. Rev. **182**, 632 (1969).
[14] R. F. Soohoo, *Theory and Applications of Ferrites* (Prentice-Hall, New Jersey, 1960).
[15] J. T. Yu, R. A. Turk, and P. E. Wigen, Phys. Rev. B **11**, 420 (1975).
[16] C. P. Hartwig, J. J. Green, R. I. Joseph, and E. Schlömann, J. Appl. Phys. **36**, 1265 (1965).
[17] R. I. Joseph and E. Schlömann, J. Appl. Phys. **38**, 1915 (1967).

Downloaded 14 Mar 2007 to 129.82.140.121. Redistribution subject to AIP license or copyright, see http://jap.aip.org/jap/copyright.jsp